ORIGINAL RESEARCH ARTICLE

Characterization and Comparison of Single VAR-Remelted and Double VAR-Remelted Ingots of INCOLOY ® Alloy 925

A. DUCOLI, D. MOMBELLI, A. GRUTTADAURIA, A. FEBBRARI, S. BARELLA, C. MAPELLI, and C. VERONESI

Alloy 925 is a nickel-based superalloy usually produced by Electric Arc Furnace (EAF), followed by Argon Oxygen Decarburization (AOD) and Vacuum Arc Remelting (VAR). It can undergo to one VAR remelting (EAF-AOD-VAR) or, if necessary due to process instabilities, two VAR remelting (EAF-AOD-VAR-VAR). The characterization of A925 ingots remelted one or two times after forging and aging was carried out to enhance differences. The VAR remelting rate of single- or double-remelted samples was correlated to metallurgical and mechanical properties. The microstructure observation revealed a higher quantity of MC, $M_{23}C_6$ and TiN precipitates (both inter- and intragranular) in single-remelted samples: the intergranular ones increase in quantity going from the ingot center position to the external one where cluster of titanium nitrides were detected. The higher presence of intergranular precipitates causes a high deterioration of impact toughness (71.1 ± 12.7 *vs* 90.5 ± 7.1 J) and lateral expansion (0.91 ± 0.18 *vs* 1.14 ± 0.07 mm). On the other hand, the number of remelting does not affect other tensile properties and hardness. Therefore, the different behavior of forged ingots at single and double remelting are not related to the number of remelting and remelting rate. On the other hand, the slightly lower toughness of single-remelted forged ingots can be corelated to defects derived from casting.

https://doi.org/10.1007/s11661-022-06815-x

I. INTRODUCTION

UNS N09925, also called Alloy 925, is a nickel–iron–chromium austenitic alloy with additions of molybdenum, copper, titanium and aluminum. Since it is a precipitation-hardenable alloy, Ti and Al are specifically added to give a strengthening of the alloy during aging, as $Ni_3(Al,Ti)$ (γ') precipitates inside the alloy matrix. Precipitation greatly increases the hardness and strength and the good mechanical resistance is in combination with excellent corrosion resistance. The addition of Cu and Mo enhances the corrosion resistance in reducing environments. Ni reduces the risk of Stress Corrosion Cracking (SCC) and the presence of Cr provides resistance in oxidizing environments. Moreover, molybdenum increases resistance to pitting and crevice corrosion, lifting the Pitting Resistance Equivalent Number (PREN) to about 31.[1,2] The combination of high strength and corrosion resistance makes it suitable in applications such as down-hole and surface gas-well components including valves, hangers, packers, and tubulars, in sour gas environments. It can also be used for fasteners, and for pump shafts in marine environments.

For production of UNS N09925, two melting stages are necessary. The primary melting is performed by the combination of Electric Arc Furnace (EAF) followed by Argon Oxygen Decarburization (AOD) refining. The remelting is performed by Vacuum Arc Remelting (VAR) and allows to improve the ingot microstructure and to reduce segregations and inclusion content.

VAR process consists in the remelting of a cast electrode using heat produced by an electric arc. Its aim is the improvement of the cleanliness and ingot structure to increase fatigue and fracture toughness of the final products. The reduction of segregations is another beneficial effect, but the homogenization of the distribution of elements is just locally due to the progressive melting of the electrode and the limited extension of the melting pool.

A. DUCOLI, D. MOMBELLI, A. GRUTTADAURIA, S. BARELLA, and C. MAPELLI are with the Politecnico di Milano, Dipartimento di Meccanica, Via La Masa 1, 20156 Milano, Italy. Contact e-mail: davide.mombelli@polimi.it A. FEBBRARI and C. VERONESI are with the Italfond S.p.A., Via Industriale 1, 25021 Bagnolo Mella (BS), Italy.
Manuscript submitted July 28, 2022; accepted August 31, 2022.

Published online: 21 September 2022

Centre porosity and typical segregations of ingot casting are eliminated due to progressive melting and solidification. The solidification structure of a VAR ingot depends on solidification rate and on temperature gradient at the interface. The direction of growth of the cellular dendrites is the same of the direction of the heat flow, which is always perpendicular to the solidification front. This brings to the formation of big central columnar grains perpendicular to the pool profile. Higher is the melting rate, deeper is the melting pool and, therefore, the grains grow tilt respect to the ingot axis. A columnar grain parallel to the ingot axis, which is the best result, can be achieved by low melting rate, but to obtain a good ingot surface a certain level of input current is required. So, the melting rate of each process must be chosen based on ingot diameter and processed metal.[3,4]

During the processing of segregation-sensitive materials, it is important to reach the steady-state condition of the solidification front avoiding its perturbation, otherwise defects can be formed.[5] This condition is met by holding the melting rate, the electrode gap, and the furnace pressure as constant as possible. The control of melting rate is very important; variations cause transients in the ingot growth and temperature gradients in the mushy zone, which lead to the formation of defects.[4] If the process is carried out in steady-state condition, the application of a constant melting power causes a constant melting rate. This relation is no more valid if there are transients in the electrode temperature distribution. These situations are typical during the start (stage 1 in Figure 1(a)) and hot-topping stages (stage 3 in Figure 1(a)), or in case of process upset, *e.g.*, pressure fluctuation due to electrode contaminations. Thus, a typical VAR remelting is a three-stage process. Also, a discontinuity in the electrode (inclusions, porosities, cracks, *etc.*) gives rise to a perturbation in the melting rate.[5] Even if the perturbation is small, numerous solidification white spots and a fine columnar structure can be seen in correspondence of a defect in a remelted ingot.[5] These defects also cause constricted arc conducive process, that induces more segregations and defects.[4] Other critical factors which influence the metallurgical structure of the final ingot are the temperature distribution and fluid motion in the liquid pool caused by the buoyancy and the Lorentz forces.[4,6]

The quality of the remelting process is evaluated by the stability of the remelting rate (in kg/min) in the second stage, which is affected by the perturbation of the steady-state condition during the remelting. Therefore, higher is the deviation of the remelting rate from the constant trend, lower is the effectiveness of the VAR process. In Figure 1 an example of a good constant remelting rate step (typical of a double remelting process) is reported in comparison to a not good one (typical of a single remelting process). It is worthy to highlight the intense fluctuation of the remelting rate during a single VAR remelting. For alloy 925, a single VAR remelting is sometimes enough to obtain a good quality ingot, *i.e.*, an ingot in compliance with API 6ACRA Standard prescriptions; while often, in the limit condition, a single remelting does not assure the wanted cleanliness level, therefore a second remelting must be necessarily performed. Thus, the purpose of this work is to understand if the mechanical and metallurgical quality of the ingots obtained after a single acceptable remelting is equivalent to the one obtained with a double remelting and if the final metallurgical and mechanical properties are affected by the remelting rates. In other words, the work aims to understand if a second remelting is always mandatory, especially when the remelting rate of a single VAR process is equivalent of the one of a double VAR process. This can conduct to a shorten of the production process and the relative costs.

II. MATERIALS AND METHODS

The nominal chemical composition of the alloy 925 is reported in Table I.[2]

For the sake of confidentiality, the actual chemical composition among the 20 investigated ingots is reported in Table II as standard deviation. The variation

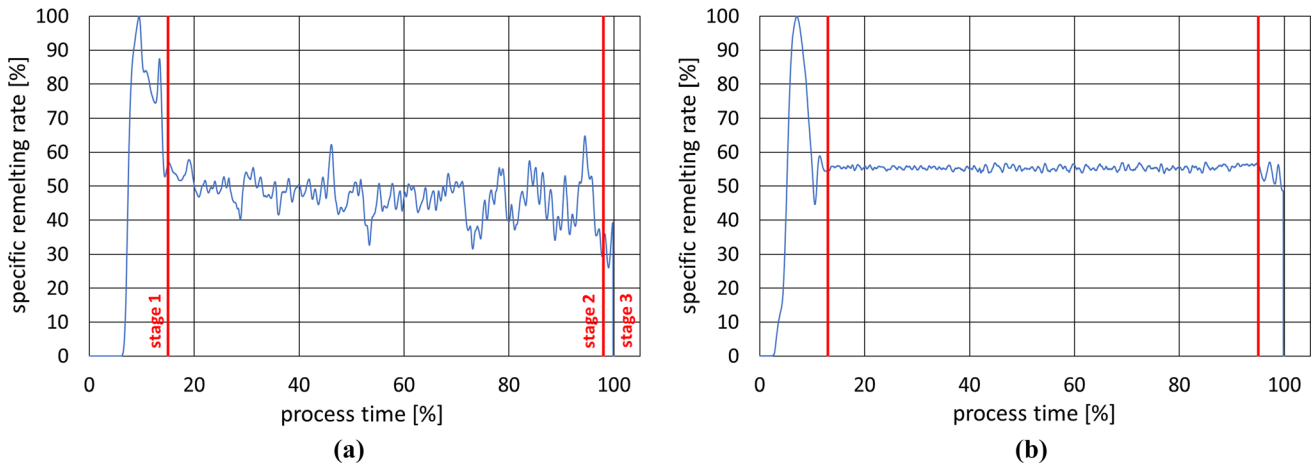

Fig. 1—Typical good trend (*a*) and typical not good trend (*b*) of the remelting rate during a VAR process.

Table I. Nominal Chemical Composition of Alloy 925 (Wt Pct)

C	Cr	Ni	Mo	Fe	Ti	Cu	Al	Nb
< 0.025	19.5 to 22.5	42.0 to 46.0	2.5 to 3.5	> 22.0	1.9 to 2.4	1.5 to 3.0	0.1 to 0.5	0.08 to 0.5

Table II. Standard Deviation of the Main Elements in Comparison with the Average Chemical Composition of All the Investigated Castings (Wt Pct)

Remelting	C	Cr	Mo	Ni	Fe	Ti	Cu	Al	Nb
Single (A)	± 0.002	± 0.16	± 0.04	± 0.43	± 0.34	± 0.033	± 0.090	± 0.02	± 0.011
Double (B)	± 0.002	± 0.14	± 0.07	± 0.32	± 0.29	± 0.036	± 0.039	± 0.02	± 0.007

of the most of chemicals is negligible and all the analyzed ingots perfectly comply with the range in Table I. From the data, a slightly lower standard deviation can be observed for double-remelted ingots. This is typical of repeated number of VAR remelting and means a higher homogeneity of double-remelted samples.[3,7–9]

10 ingots single-remelted (group A) and 10 double-remelted (group B) are selected from 2020 production. All the analyses are performed on final products, therefore after forging, solution annealing and aging. This choice follows twofold reasons. Single-remelted ingots that comply with API 6ACRA Standard are considered satisfactorily, hence salable. Secondarily, quality characterization is performed on the final product only, as per internal practice of the company. The VAR-remelted ingot are generally forged in the range 870 °C to 1100 °C and then solubilized at 1010 °C for 2 h, followed by a water quenching. A stepped aging is performed by maintaining the solubilized ingot at 740 °C for 9 h followed by an oven cooling to 621 °C and a further maintaining for 9 h. Final cooling is performed in air. To have comparable mechanical properties, all the investigated ingots have a similar reduction ratio, they are derived from 560 mm VAR crucible diameter, and they were in agreement with the prescriptions of the API 6ACRA Standard "Age-hardened Nickel-based Alloys for Oil and Gas Drilling and Production Equipment."[2]

The samples undergo characterization are extracted from the so-called Qualification Test Coupons (QTC), which are specimens prepared from an extension of the final product (full cross-section on thickest end) or from a sacrificial product part. For forged bars, a slice 140 mm high is cut from the head of ingot (below the hot-topping zone, Figure 2).

Micrographic examination is performed on polished samples by an Olympus BX61 light microscope. To evaluate the grain size and secondary phases, etching by Kalling's No. 2 (5 g $CuCl_2$, 100 mL HCl, 100 mL ethanol) is performed. The observation is done on central, mid radius and external position. One sample per each zone was investigated, according to the internal practice of the company (Figure 2). The precipitation at grain boundary is estimated by the ratio between the precipitated and the overall area of the microscopy image. The analysis is performed on etched samples from mid radius position at 100X magnification by ImageJ software. The percentage of area occupied by the precipitate is calculated and converted in mass percentage by Eq. [1], as suggested by Berthod *et al.*[10]

$$f_{mass}(\varphi_j) = \frac{\rho_{\varphi_j} \cdot f_{vol}(\varphi_j)}{\sum_i \rho_{\varphi_j} \cdot f_{vol}(\varphi_j)} \quad [1]$$

where $\rho_{\varphi j}$, $f_{mass}(\varphi_j)$ and $f_{vol}(\varphi_j)$ are, respectively, the density, the mass fraction, and the volume fraction, which is approximatively equal to surface fraction, of the considered phase φ_j. However, the calculation of percentage area of precipitates does not allow to discriminate different particles, therefore only the $Cr_{23}C_6$ densities, which is the more representative, is used.

Scanning Electron Microscope is used for the morphological characterization of precipitates, *via* secondary electron (SE) and backscattered electron (BSE). Energy dispersive spectroscopy (EDS) probe is used to reveal precipitates composition. The combination of EDS analysis and precipitates morphology found in bibliography allows to establish their nature. A Zeiss Sigma 300 Field Emission Scanning Electron Microscope (FEG-SEM) coupled with an Oxford Xmax Ultim 65 EDS probe was employed.

X-ray Diffraction (XRD) analysis is performed to detect eventually secondary phases. The test is performed using a Rigaku SmartLab SE diffractometer equipped with copper tube (λ = 1.54 Å). A bulk sample is scanned from 20 to 100 deg 2θ at 1 deg/min with 0.02 deg step size. A 1D D/Tex Ultra 250 detector with energy fluorescence suppressor is used to acquire the diffracted beam. The analysis is performed on two sets of three samples (center, mid radius and external position of QTC) for single and double-remelted. The XRD detection limit is about 3 to 4 wt pct.

Three tensile tests per each ingot are performed by Z250 Zwick/Roell static testing machine. According with API 6ACRA[2] samples are obtained longitudinally from the mid radius position of the QTC (Figure 2). The test is conducted at room temperature following the test

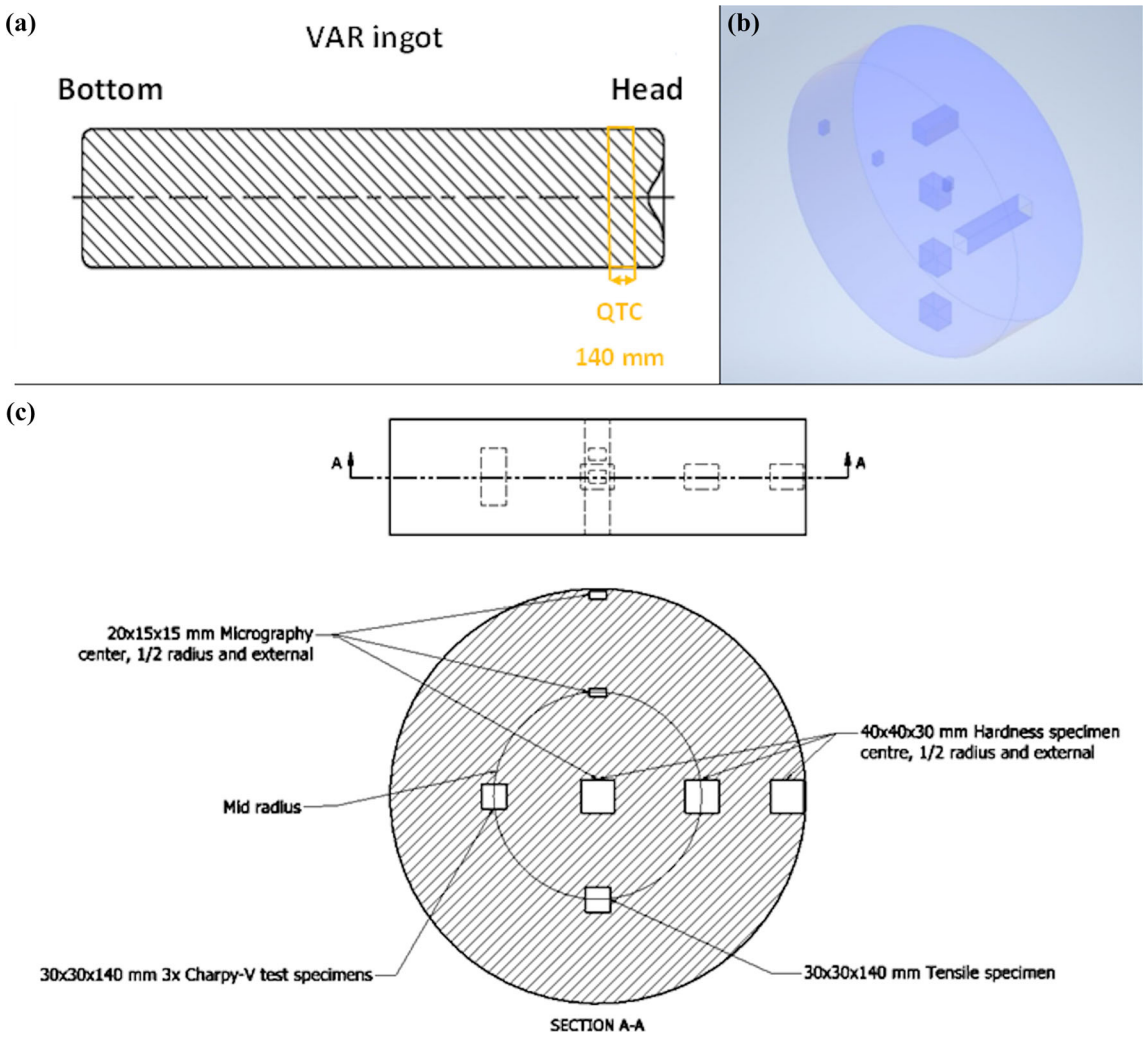

Fig. 2—QTC location in a VAR ingot (*a*). 3D representation of specimen positions in QTC (*b*). Scheme of specimens' location and size in QTC (*c*).

method reported in ASTM A370 at a speed equal to 2 mm/min.

Charpy impact test allows to determine the amount of energy absorbed by the specimen during the fracture (toughness of the material), the lateral expansion of the sample, and the shear fracture. The pendulum impact tester used is the PSW750 Zwick/Roell. The test was performed on V-notch samples, in accordance with ASTM A370, and at temperature − 60 °C. Three specimens for each ingot with transverse orientation (parallel to the ingot axis) undergo to the test (Figure 2).

Hardness test is performed using Rockwell C-scale method, per ASTM E18 or ASTM E110, and the Brinell (10 mm ball, 3000 kgf) method, per ASTM E10 or ASTM E110, after the final heat treatment.

Rockwell C-scale test is performed by Zwick-Roell ZHR durometer, making three adjacent indentations. Also, for Brinell test three indentations are performed. The apparatus used is 3000BLD/T durometer of Wolpert Wilson Instruments. The measurements are performed on three zone of the ingot cross-section: the center, mid radius and near surface.

Mechanical properties results are statistically compared by the Honest Significant Difference (HSD) Tukey's test, which is part of the Analysis of Variance (ANOVA), to demonstrates if the series are significatively different.[11]

The method consists in the calculation of the Honest Significant Difference (2), which depends on the variance of the series by the Mean Square Within (3) and their population, then the difference between the mean values of the two series is compared with it. If the difference is lower than the HSD, the series are statistically equal.

$$HSD = q * \sqrt{\frac{MSW}{n}} \qquad [2]$$

where q is a constant (which depends on N, k and significance) from q table, MSW and the lower n of the analyzed series.

$$MSW = \frac{\sum_{i=1}^{k}(n_i - 1)s_i^2}{N - k} \qquad [3]$$

where s^2_i is the variance of the single series, n_i is the number of measures in the single series, N is the total measures in all series and k is the number of series.

95 pct confidence interval (CI) for the mean (4) based on standard error (5) of each samples group (A and B) are also graphically represented both for single (s) and pooled variance (s_p) (6). Due to the fact that the number of samples considered is highly below 100, therefore with few degrees of freedom, and the variance is estimated from sample data, the t-Student distribution must be used instead of the normal distribution.[12]

$$CI = \pm t_{0.95} SE \quad [4]$$

$$SE = \frac{s}{\sqrt{n}} or \frac{s_p}{\sqrt{n}} \quad [5]$$

$$s_p = \sqrt{\frac{(n_1 - 1)s_1^2 + (n_2 - 1)s_2^2}{n_1 + n_2 - 2}} \quad [6]$$

III. RESULTS

The reduction ratio of the diameter of the ingot after forging is calculated. The average final diameter and reduction ratio, calculated as the ratio between the starting section area and the final area, are, respectively, 181.8 mm and 11.0 for single-remelted ingots (A), while they are 188.0 and 9.4 for double-remelted ingots (B). Therefore, the experimental results can be compared, even if single-remelted ingots have slightly higher reduction ratio. The analysis of the remelting rate and its deviation pointed out a slightly higher deviation for single-remelted ingots (+ 36 pct) that results in a + 12.5 pct in the remelting rate than ingots B. This directly depends on the different internal quality of the electrode (respectively casting ingot and single-remelted ingot).[4,5] However, since all the ingots A comply with the API 6ACRA requirements, if no significant difference will be highlighted by the metallurgical and mechanical comparison among the two groups, a faster and economic production can be expected.

A. *Microstructural observation and precipitates characterization*

The observation of non-etched samples by optical microscope reveals the presence of titanium nitrides, recognizable by their polygonal shape and orange-yellow color (Figure 3(a)). The presence of these precipitates is expected because EAF, AOD and casting are performed in natural atmosphere, therefore, rich of nitrogen which diffuses inside the metal mass. Moreover, the addition of titanium before casting, to achieve the desired composition, enhances the formation of titanium nitrides, due to its high reactivity. During VAR process, they dissolve and the quantity of the nitrogen present in the alloy is highly reduced. The first metal solidified on the water-cooled crucible has a low solute content; this outer layer is called "shelf". During the remelting due to lower density, inclusions, highly stable oxides, carbides, and nitrides are swept to the top of the molten pool and they are incorporated into the shelf tanks to the pool shape. Less stable oxides and nitrides are thermally dissociated or reduced by carbon in the alloy, and they are removed by gas phase.[7,13] Despite this, titanium nitrides nucleate again thanks to nitrogen micro-segregation, but the total amount of this precipitate becomes lower and lower at every VAR remelting.[7,14] In addition, aging may also stimulate the formation of TiN, as reported by Ganesan *et al.*[15]

Lot of titanium nitrides has a central dark spot, as can be seen in Figure 3. The EDS analysis reveals they are particles of MgO (Figure 3), and therefore, it acts as nucleating site for titanium nitrides. Magnesium oxide can derive from refractory, slag or final reduction of the heat by NiMg. The latter is more probable because slag is removed before the transfer of the bath in the ladle and the NiMg is the last addition before the casting. Therefore, magnesium reacts with oxides forming MgO. The nucleating effect of Mg oxide (periclase, spinel, *etc.*) was observed in other INCOLOY grades.[16] The originated nitrides sometimes act as nucleating for carbides.[14] This phenomenon can be seen by optical microscope images where orange titanium nitrides are surrounded by a dark layer, which is composed by carbides (Figure 4).

These titanium nitrides are homogeneously distributed in central and mid radius position in both single and double-remelted ingots. In central position, nitrides are few and all about 10 μm length. Moving to the outer part of the ingot, the distribution of nitride dimensions becomes wider up to 16 μm. In external position, clusters of nitrides oriented in the forging direction are revealed in single-remelted samples (Figure 4). The double-remelted samples show a general lower presence of precipitates. In the external zone of double-remelted specimens, a homogeneous distribution is detected, with exception of few little groups of precipitates. Moreover, especially for the double-remelted samples, it is not unusual to find field completely without nitrides, while in single-remelted specimens, titanium nitrides are more abundant and the worst situation is represented by the external zone.

After etching, both the microstructure and the position of the different precipitates is revealed. The average grain size of the nickel matrix is calculated by intercept method according to the standard ASTM E112, and an average grain dimension of about 89.8 μm was obtained.

By means of the analysis on grain boundary precipitates it is possible to assess the area of micrograph occupied by other precipitates than nitrides. In single-remelted specimens, it is 5.70 ± 2.69 pct, while in double-remelted ones it is 2.01 ± 0.087 pct (Figure 5). In single-remelted samples grain boundaries are more marked and thicker than the double-remelted, meaning that they are more precipitated and so more prone to corrosion.

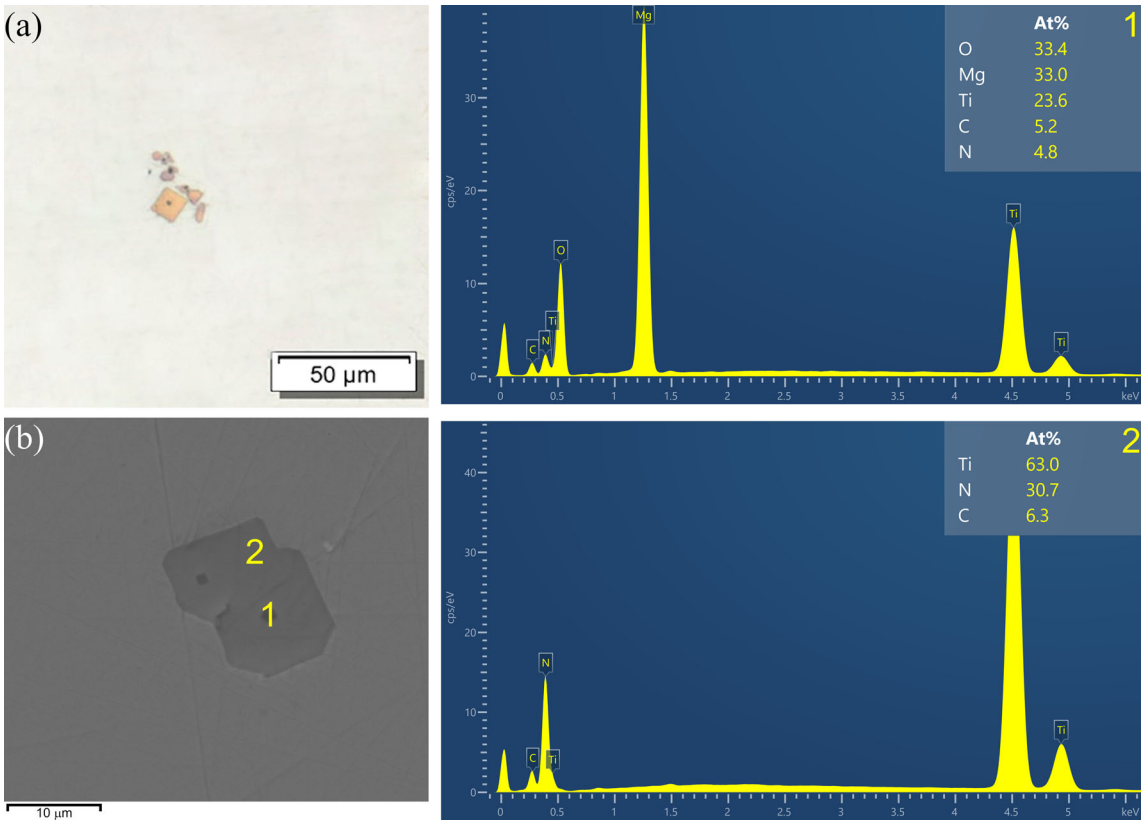

Fig. 3—Cluster of titanium nitride in external sample of single-remelted ingot (optical microscope) (*a*). Titanium nitride with MgO core (SEM) (*b*). 1 and 2 are EDS in atomic percentage (Color figure online).

To have a first confirmation about the different rate of precipitation in both the samples group (A and B), a XRD analysis was performed. The limit of detection (LOD) of such a technique for the experimental setup chosen and equipment performance is roughly 3 to 4 wt pct. Therefore, the expected secondary phase content of double-remelted samples is below the LOD, while the estimated fraction for single-remelted specimens is close to the LOD. As expected, no peaks of secondary phases are revealed in double-remelted samples in all positions, since only the peaks of nickel can be detected. Instead, secondary phase peaks are detected in a single-remelted sample (Figure 6). From bibliography,[17–19] peaks at the left of the principal nickel peak, indicated by the arrows, can be associated to carbides. Due to the complex and variable composition of $M_{23}C_6$ and M_6C, the association of each peak is not easy and not possible using the reference pattern within the COD (Crystallographic Open Database). However, the presence of peaks at larger angles (between 60 and 80 deg 2θ) can suggest they belong to TiN.[20] Therefore, the comparison of XRDs with the ones of other superalloys and with SEM observation can give an idea of the quality of precipitates. Despite, XRD spectra clearly show the increasing of precipitates from the center to the external position in single-remelted samples.

As can be seen from Figure 7, SEM images confirms the different quantity of precipitates at grain boundaries of single-remelted ingots and double-remelted ingots. In particular, center position of single-remelted ingot (Figure 7(a)), corresponding to the best position at cleanliness level, is compared with the external position of the double-remelted ingot (Figure 7(d)) that correspond to the worst position. At exception of intragranular precipitates, which are a peculiarity of the process in the external part of the ingot, the intergranular precipitation is lower in double-remelted specimens. Generally, single-remelted samples have bigger and more diffused grain boundaries precipitation respect to double-remelted specimens. Moreover, the latter does not show important qualitative difference between center, mid radius and external zone, while single-remelted samples have an increasing quantity of molybdenum rich precipitates, MC carbides and cluster of titanium nitrides, in the intragranular zone from the center to the external specimen (worst situation). This difference can be noticed from Figure 7(a) through (c), in which the center, mid radius and external SEM micrographs are reported, respectively. The external sample is the most precipitated with chains of M_2C carbides and clusters of titanium nitrides (Figure 8(b)). M_2C mainly contain molybdenum, chromium and a small concentration of nickel, and they form spherical shape particles organized in strings. They precipitate preferentially at grain boundary during the initial stage of thermal treatment, then they transform into massive

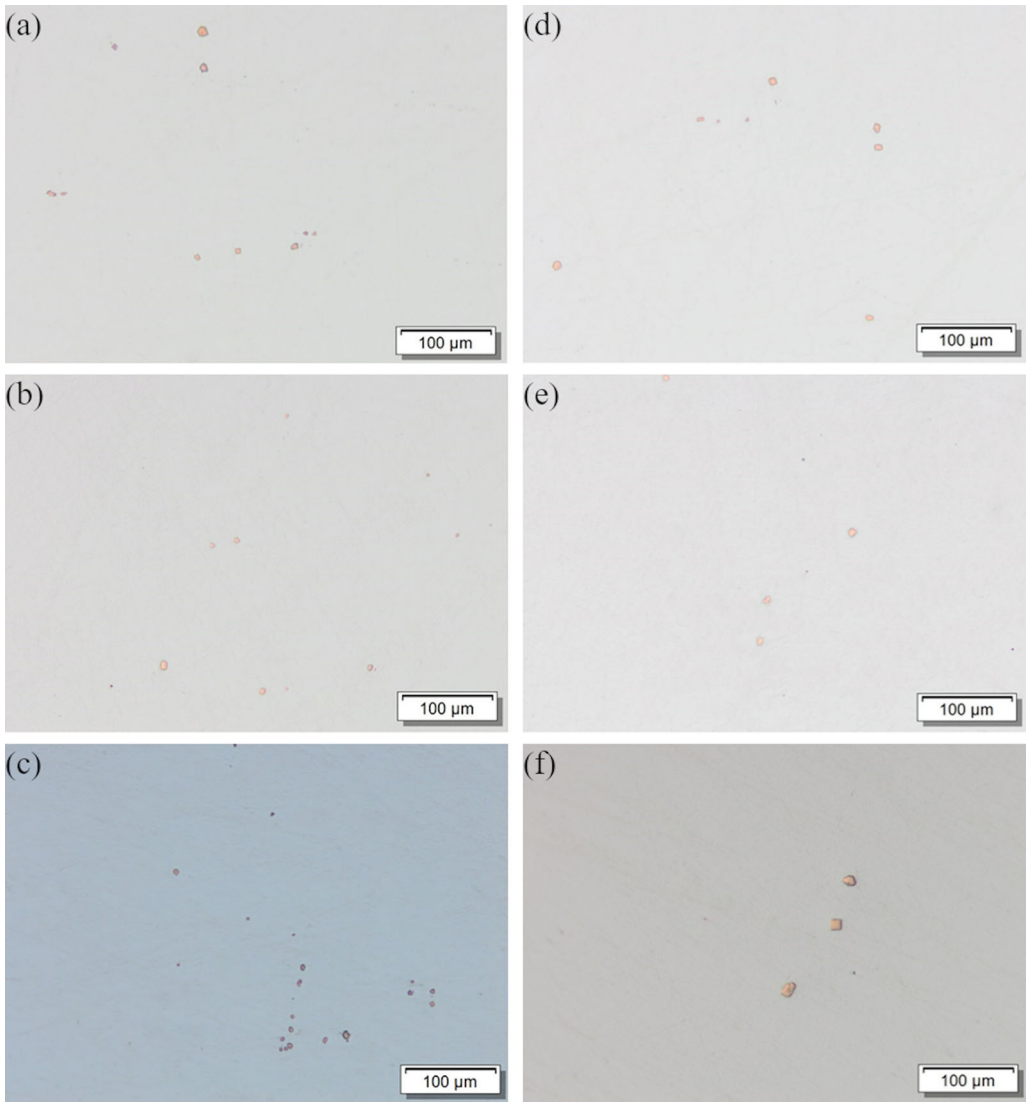

Fig. 4—Worst fields of single-remelted samples at (*a*) center, (*b*) mid radius and (*c*) external) and double-remelted ones at (*d*) center, (*e*) mid radius and (*f*) external). Optical microscope.

plate-like M_6C as the aging time increases. This transformation is controlled by Si and it is favored at high Si concentration.[21,22] Otherwise, M_2C can precipitates in correspondence of dislocation within the matrix and in specific condition (solution treating followed by low-temperature aging) they coherently precipitate intragranularly.[23–26] This latter behavior seems what happened in the A925 under investigation. Indeed, the VAR ingots undergo solution treating and annealing after hot forging. This creates a favorable condition for M_2C intragranular precipitation. In addition, the low Si of the A925 alloy (< 0.35 wt pct) partially inhibits the $M_2C \rightarrow M_6C$ transition. The presence of M_2C carbides can be also confirmed by the three typical peaks in the range 30 deg to 40 deg 2θ detected in Figure 6.[27,28] Precipitates at grain boundaries are generally Cr-enriched $M_{23}C_6$ (Figures 8(a) and (d)), while Mo and Cr-enriched M_6C can be found both in intragranular and intergranular position (Figure 8(c)). The presence of such precipitates, mainly TiN and $M_{23}C_6$, is a consequence of the aging treatment. As reported by Ganesan *et al.*, in the thermal range 732 °C to 760 °C, the precipitation of MC, TiN and M_7C_3 is foreseen for an aging of 8 h.[15] Lowering the temperature, also $M_{23}C_6$ forms. Because of M_7C_3 are metastable, they transform in $M_{23}C_6$ during heat treatment.[7,29,30] Being the aging executed in two steps (the former at 740 °C and the latter at 621 °C) both lasting 9 h, current findings and literature are in good agreement.

To summarize, all the different second phases detected are reported in Table III with their average dimension. All those phases are detected in both single-remelted and double-remelted sample, but in different amount.

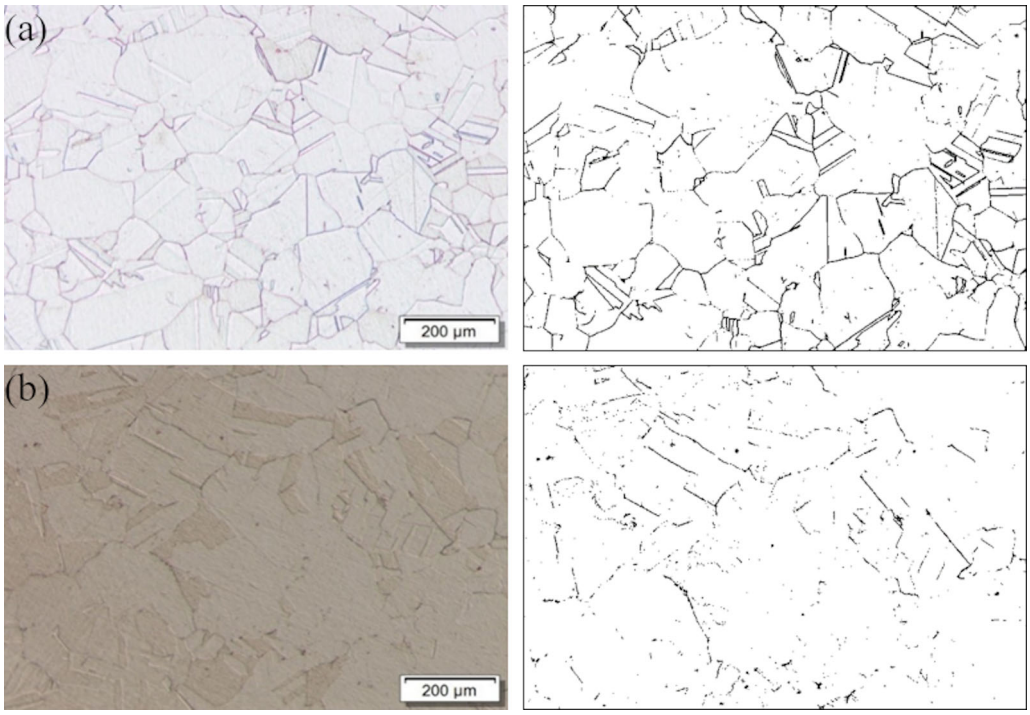

Fig. 5—Micrography of etched samples (left) and ImageJ pictures with threshold (right) of a single-remelted (precipitates fraction 6.86 ± 0.25 pct) (*a*) and a double-remelted (precipitates fraction 1.45 ± 0.25 pct) (*b*) samples.

B. *Mechanical Characterization*

The results of Charpy test on sample A (single-remelted) and sample B (double-remelted) are reported in Table IV. The average fracture energy of double-remelted specimens is about 19.4 J higher than the one of single-remelted samples. Contextually, even the average lateral expansion of double-remelted sample is higher than single-remelted one. Therefore, double-remelted samples seem to be more tough and ductile than single-remelted ones. The shear fracture area is 100 pct for all samples, which is typical of superalloys.

About tensile tests, all the mechanical properties do not seem to have remarkable differences both in average value and standard deviation, as can be seen in Table V. An example of tensile curves is reported in Figure 9. From the graph, no macroscopic differences can be highlighted between the two group of ingots as well as the high control of the VAR process is reflected in a very low scattering of the curves belonging the same ingot. Quantitatively, the standard deviation among the three tensile specimens is always below the measurement uncertainty. Therefore, uncertainty is used to express the measurement variability.

Results of hardness tests are reported in Table VI. No differences can be appreciated, especially for Rockwell hardness. In fact, the single-remelted specimens and double-remelted ones show the same average values of the latter. Charpy toughness and elongation show values in line with the literature for similar aged A925, while the current forged ingots exhibited higher strength (+ 18–20 pct) and less ductility (− 25 pct).[15]

IV. DISCUSSION

Thanks to the observations at optical microscope of non-etched samples, it was possible to assess that single-remelted samples contain a higher amount of titanium nitride respect to the double-remelted ones. It agrees with the specificity of the production process. For instance, one of the advantages of VAR remelting is the possibility to dissolve part of the nitrides, due to the low initial concentration of nitrogen in the cast alloy. Therefore, a part of nitrogen is removed during the first VAR remelting.[14] Then, the nitrides precipitate again thanks to solidification-induced segregation, but in lower quantity than before due to the lower amount of nitrogen in the alloy. Furthermore, the non-dissolved titanium nitrides are dragged by pool flow to the skin of the ingot, where they are incorporated and removed once the process is ended.[7] This happens at every VAR remelting stage. Obviously, if the VAR process will be performed another time, the reduction of nitrogen and, therefore, of titanium nitrides will be higher. Another difference between the two processes is the presence of titanium nitride clusters in the external sections of single-remelted ingots. As reported in literature, they can act as crack initiation in fatigue tests.[31,32] Therefore, they can be detrimental in the fatigue property of parts produced from that kind of ingots, especially if they are hollow. The presence of clusters in the external part can be justified by the pool flow. Non-dissolved nitrides tend to be dragged toward the skin, but if they do not reach it, they are trapped in the mushy zone of the external zone of the ingot, where they release

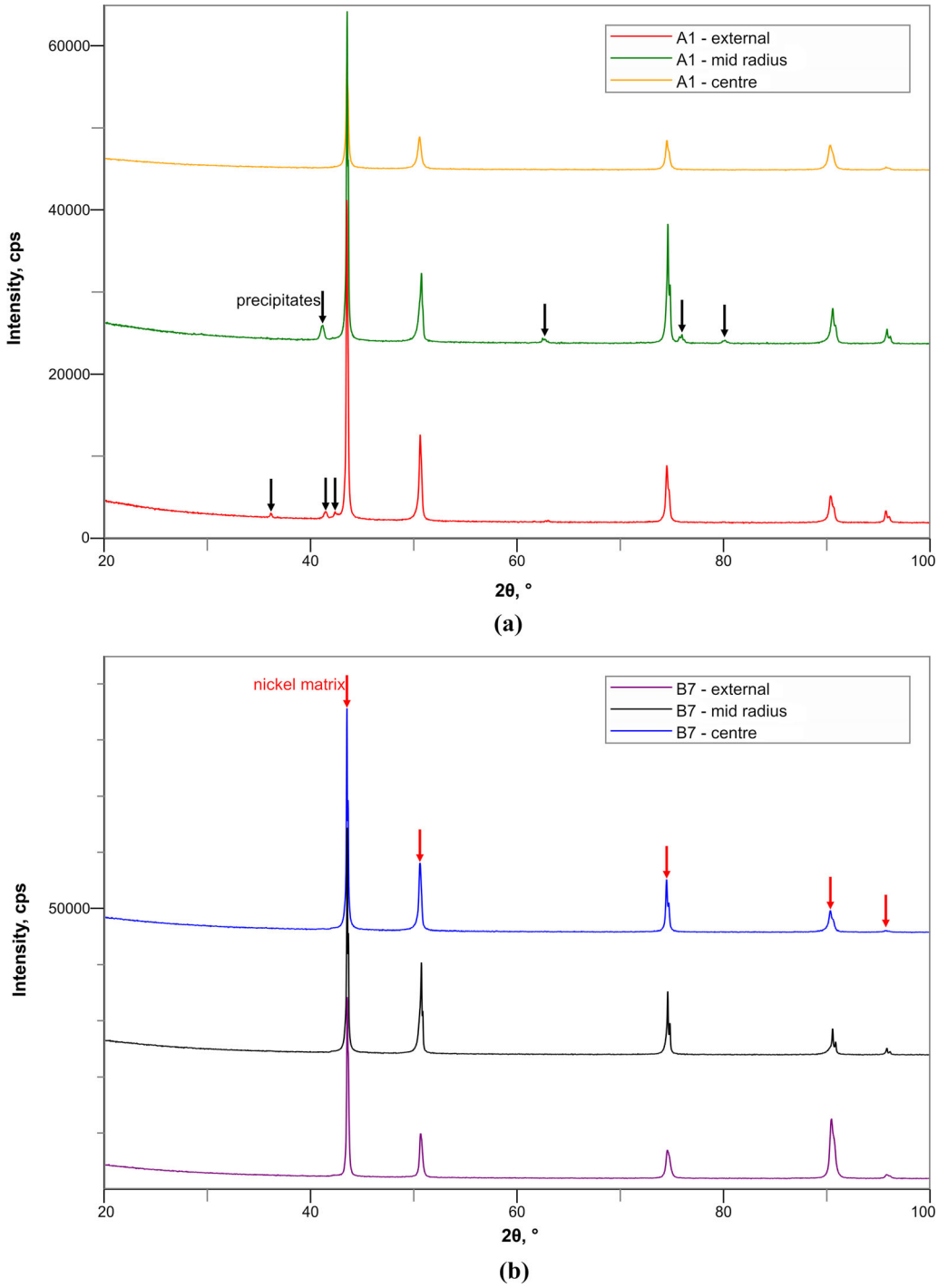

Fig. 6—XRD patterns of (*a*) single-remelted sample; (*b*) double-remelted sample.

nitrogen and titanium in the liquid due to the changed equilibrium of the reaction. Therefore, the external part of the ingot becomes richer of nitrogen and, so, of titanium nitrides, which precipitate again due to solidification-induced segregation. Then, the forging causes the alignment of titanium nitrides cluster along the axis.[33,34] Moreover, MgO acts as nucleating for titanium nitrides, therefore the addition of NiMg as de-oxidizing agent in the ladle, before the casting and after the titanium addition, could enhance the nucleation and grow of this kind of inclusions. Data from Charpy impact test are analyzed by the Tukey test, which confirms the differences between the toughness and lateral expansion of the single-remelted and double-remelted samples. In Figure 10, the graphical representations of results of the test (Table IV) are reported in

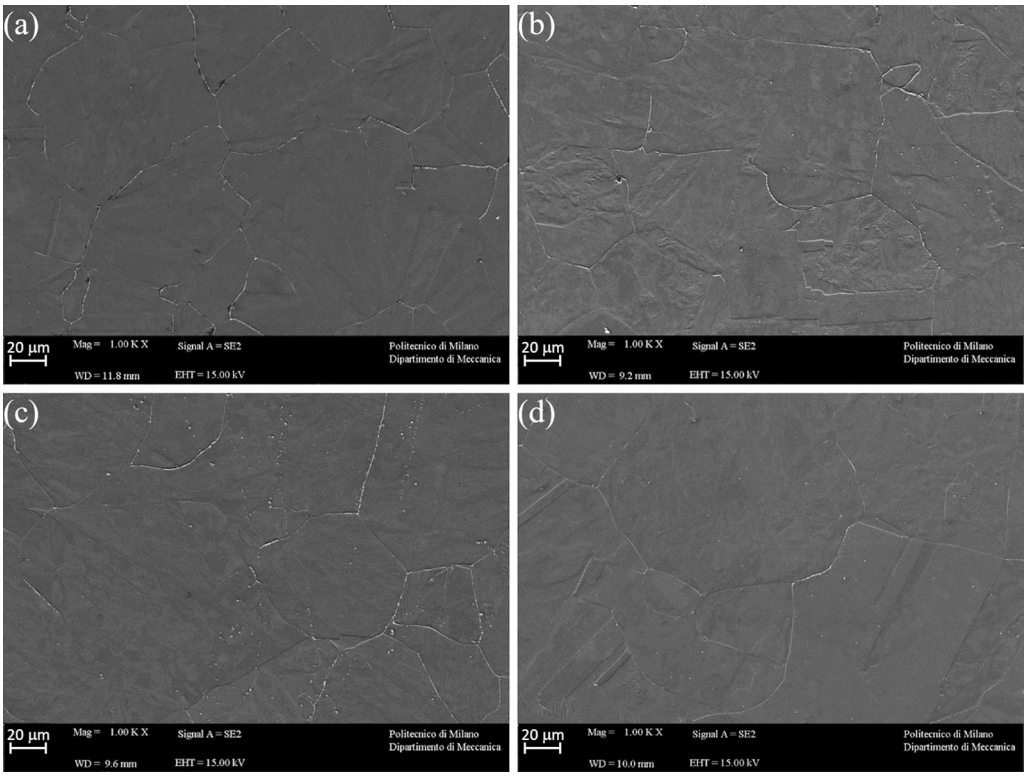

Fig. 7—Typical SEM images of single-remelted sample (*a*) center, (*b*) mid radius, (*c*) external position and (*d*) double-remelted sample in external position.

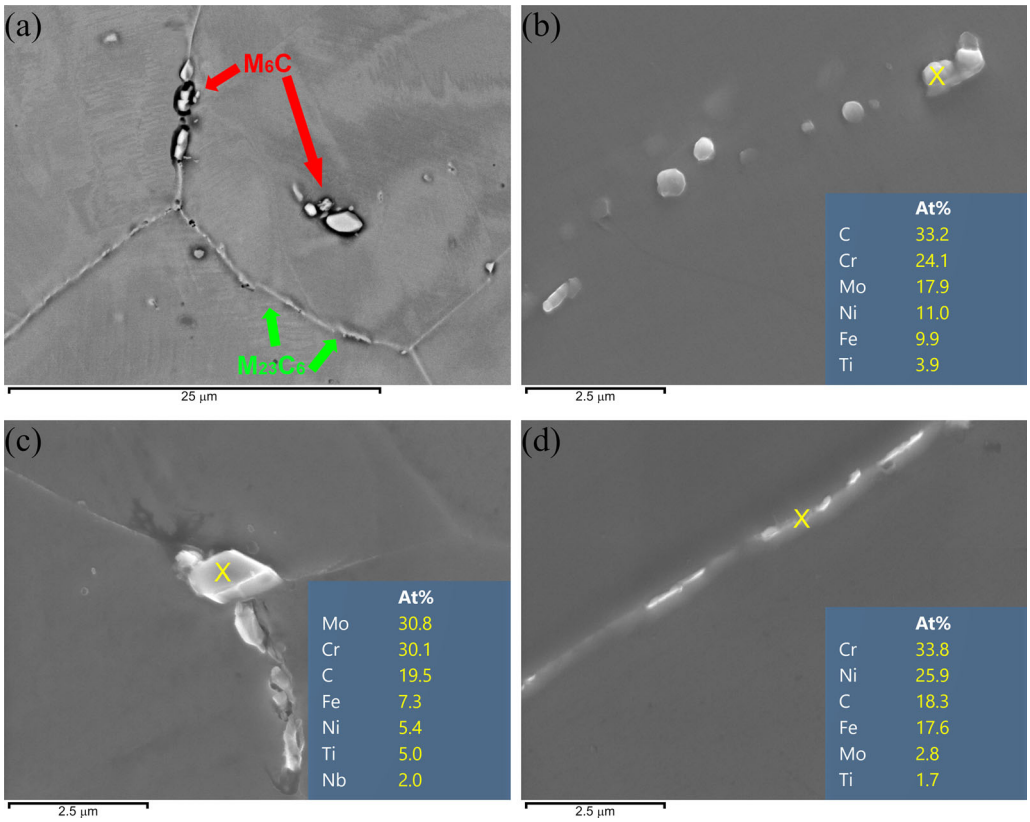

Fig. 8—Different types of carbides detected: (*a*) typical position; (*b*) M_2C; (*c*) M_6C and (*d*) $M_{23}C_6$.

Table III. Dimension and Position of Detected Secondary Phases and Precipitates

Phase	Detected	Typical dimension	Position	Sample set	Quantity
MC	Yes	400–600 nm	mainly intragranular	single/double	low/low
M_6C	Yes	2 μm	both	single/double	low/very low
$M_{23}C_6$	Yes	0.5–1 μm	mainly intergranular	single/double	relevant/low
M_2C	Yes	400–500 nm	intragranular	single/double	low/ very low
TiN	Yes	3–16 μm	mainly intragranular	single/double	relevant/less relevant
TiN + MC	Yes	3–16 μm	mainly intragranular	single/double	relevant/less relevant
Θ	No				
Σ	No				
Laves	No				

Table IV. Charpy Impact Test results for Single-Remelted Samples (A) and Double-Remelted ones (B)

	Charpy toughness (KV) [J]		Lateral expansion [mm]		Shear fracture [Pct]	
	A	B	A	B	A	B
Average	71.1	90.5	0.91	1.14	100	100
Stand. Dev	12.7	7.1	0.18	0.07	0	0

Table V. Tensile Test results for Single-Remelted Samples (A) and Double-Remelted Ones (B)

	R_{P02} [MPa]	R_{P1} [MPa]	R_m [MPa]	Elongation [Pct]	Reduction of area [Pct]
A					
Average	836	913	1158	28.3	39.8
Stand. Dev	20	17	9	1.2	2.3
B					
Average	825	904	1155	29.3	38.3
Stand. Dev	18	22	18	1.4	1.1

Yield strengths and ultimate tensile strength are calculated imposing E = 199 GPa.

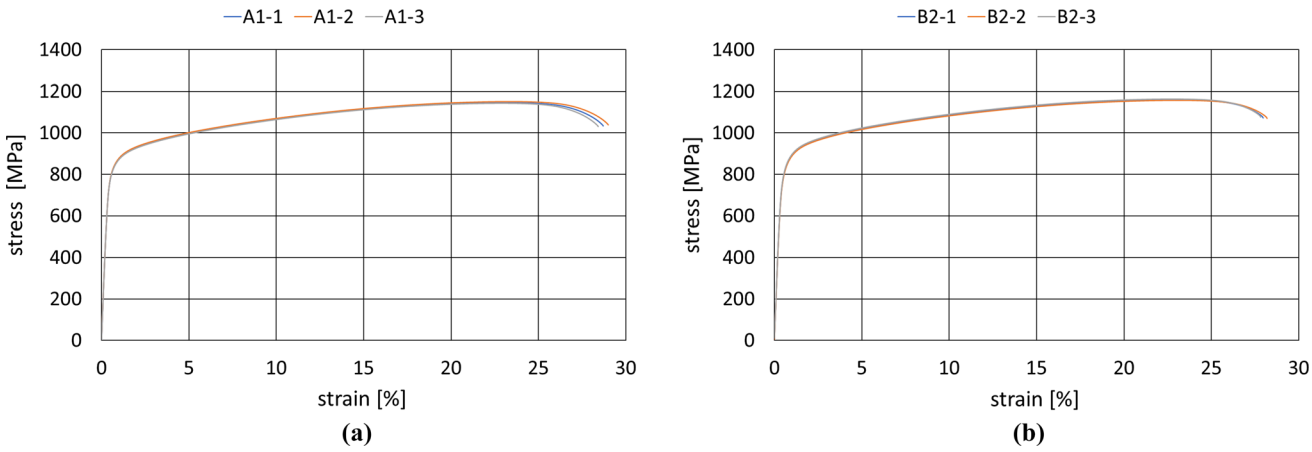

Fig. 9—Example of tensile test curve for single (sample A1) and double (sample B2) remelted ingots.

Table VI. Brinell and Rockwell Hardness of Single-Remelted Specimens (A) and Double-Remelted Specimens (B)

	A		B	
	Average	Stand. Dev	Average	Stand. Dev
HB				
Center	325.64	9.14	326.9	6.89
½ radius	325.21	9.28	327.5	6.74
External	325.04	9.97	326.4	5.96
HRC				
Center	33	1.7	33	0.7
1/2 radius	33	1.8	33	0.6
External	32	1.6	32	0.9

terms of Charpy toughness and lateral expansion. In Figures 10(a) and (b) the interval plot of the 95 pct confidence intervals calculated using the individual standard deviation are reported, while, in Figures 10(d) and (e) the HSD Tukey's test can be found. The 95 pct confidence intervals do not overlap, which means that the two series are not comparable, in according with the HSD Tukey's test results.

Another relevant observation is the difference in the standard deviation between the two different processes, which results in different confidence interval calculated with individual values. In fact, the toughness and shear fracture standard deviation of single-remelted specimens are, respectively, 12.7 J (17.8 pct) and 0.18 mm (19.38 pct), while for the double-remelted ones they are, respectively, 7.1 J (7.9 pct) and 0.07 mm (6.46 pct). From these values it can be stated that the second remelting allows to achieve more constant results, while after the first remelting, even if the process is acceptable, the toughness and lateral expansion vary on a wider range. This can be related to the different quality of the starting ingot that highly affect the quality of the remelted ingot. In fact, the first remelting is highly dependent on the cast ingot quality, while the second process remelts a more homogeneous electrode ideally without internal cavity or cracks. Therefore, the second remelting generally gives rise to less oscillating quality of the material. Moreover, by optical microscope observation, the samples with less toughness and less lateral expansion show a higher presence of carbides at grain boundaries respect to the one with higher values, observation that is in accordance with literature.[35,36]

The major area occupied by precipitates is represented by the ones located at grain boundaries. As anticipated, a relation with toughness can be noticed from Figure 11. For instance, specimens with higher percentage of precipitates show less absorption of energy at impact. Tukey's test confirms the statistical difference of precipitation between the two samples (Figures 10(c) and (f)). From literature is known that precipitates at grain boundaries, in particular $M_{23}C_6$, causes the embrittlement due to a loss of cohesion and, therefore, a preferential path for crack propagation reducing the energy necessary for sample rupture.[35,36]

The higher content of precipitates at grain boundary is due to the less cleaning effect of single remelting compared to the double. Inclusions, carbides, and other defect are dragged by pool flow to the shelf, where they are trapped. If the electrode is almost regular and homogeneous with low quantity of inclusions, *i.e.*, second remelting or high-quality casting ingot, the mechanism is very effective, therefore most of inclusions are incorporated in the shelf. Otherwise, a high-content inclusions and defects electrode does not allow an elevated cleaning effect due to the irregular remelting rate, which produces modification of pool parameters. In particular, primary carbides (MC), which form during casting, tend to transform into $M_{23}C_6$ at grain boundaries during heat treatment, if they are not trapped in the shelf.[29] Therefore, the higher precipitation in single-remelted ingots can be justified by the lower removal of primary carbides due to the single VAR process. In fact, in single-remelted sample, the intragranular precipitates increases from the center (Figure 7(a)) to the external part (Figure 7(c)), justifying the same tendency of the intergranular ones. This trend can be also appreciated by the XRD of a single-remelted sample (Figure 6). In fact, in center position no secondary peaks are present, but moving to the outer zone of the ingot they increase, consistently with the microscopical observation. Therefore, lower is the cleaning effect of the VAR process, higher will be the precipitates at grain boundaries.

Differently, tensile test results do not show differences between single-remelted samples and double-remelted ones. The interval plots of the confidence interval calculated using both individual and pooled standard deviation are reported in Figure 12. The individual standard deviations do not show a remarkable difference between the two series; therefore, the confidence intervals have similar extension. Moreover, all confidence intervals overlap, therefore the series are similar, as can be confirmed by Tukey's test.

Despite the statistical similarity of values, the slightly higher tensile properties of single-remelted samples, at exception of elongation, can be justified by the slightly higher forging reduction ratio. Indeed, considering the same material and process, yield strength, elongation and reduction area grow proportionally with respect to the reduction area, while ultimate tensile strength remains constant. Only the elongation is lower in single-remelted samples, probably due to the higher presence of precipitates which act as void-nucleating points.[37–39]

The non-influence of grain boundary carbides on ultimate tensile strength is reported by Wang *et al.*[36] and Chen and Gan,[35] which analyze, respectively, the effect of grain boundary $M_{23}C_6$ carbides in high nitrogen austenitic stainless steel and AISI 316 stainless steel. In both works, despite a severe reduction of impact properties, only a moderate reduction in elongation to rupture is observed. Both effects are noticed also in Alloy 925, even if the difference of the latter has not statistical meaning, probably due to the compensating effect of the slightly higher reduction ratio.

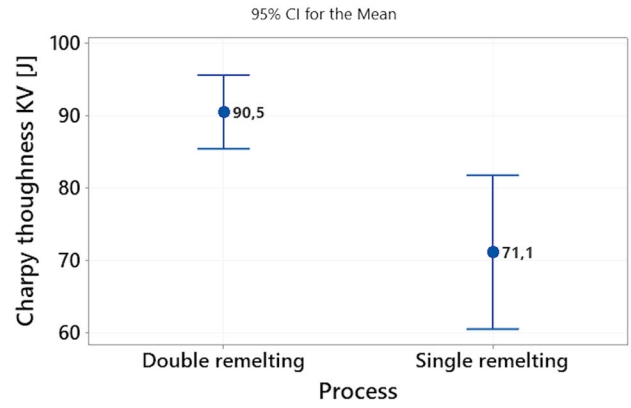

Individual standard deviations are used to calculate the intervals.

(a)

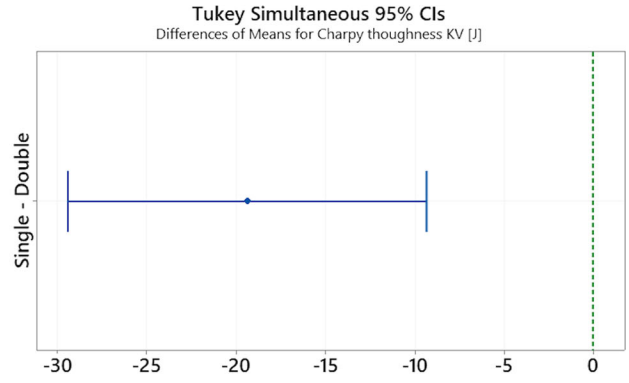

If an interval does not contain zero, the corresponding means are significantly different.

(d)

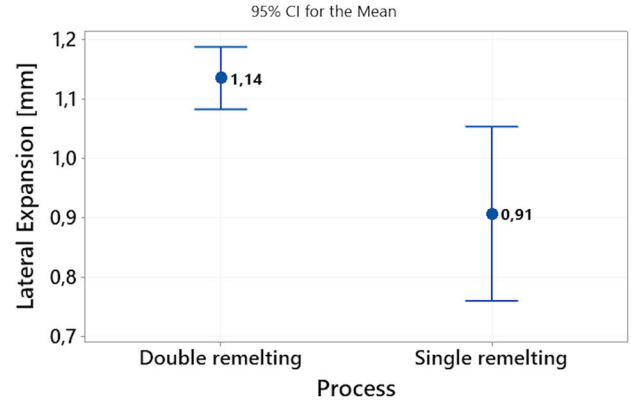

Individual standard deviations are used to calculate the intervals.

(b)

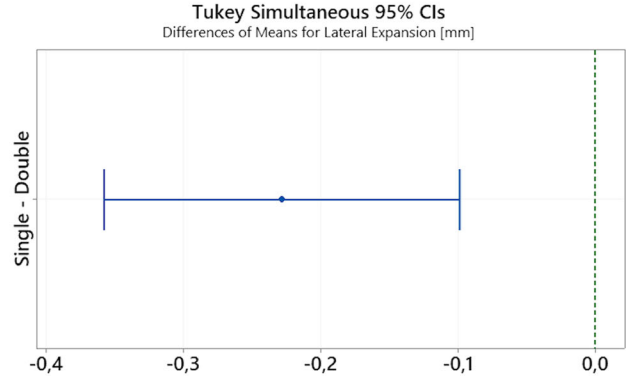

If an interval does not contain zero, the corresponding means are significantly different.

(e)

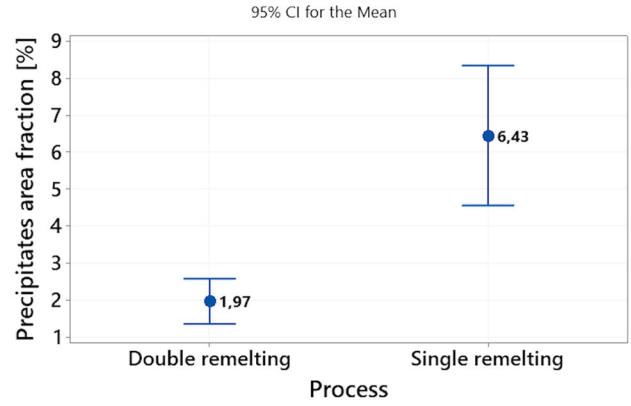

Individual standard deviations are used to calculate the intervals.

(c)

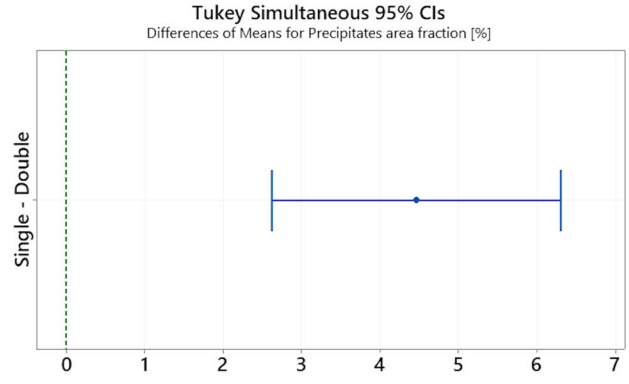

If an interval does not contain zero, the corresponding means are significantly different.

(f)

Fig. 10—Interval plot with individual standard deviation of Charpy toughness (*a*); lateral expansion (*b*); precipitates area fraction (*c*); and HSD Tukey's test plot of Charpy toughness (*d*); lateral expansion (*e*); precipitates area fraction (*f*).

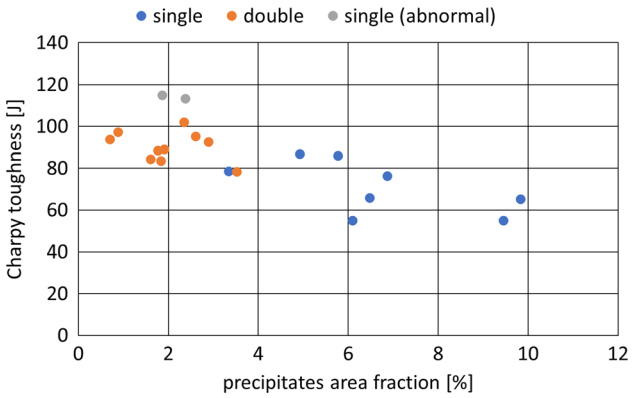

Fig. 11—Charpy impact toughness (dev.st ± 8.3 J) *vs* precipitates area fraction (dev.st ± 0.25 pct).

The different influence of precipitates at grain boundary between impact test and tensile test can be justified also considering that the latter is a quasi-static test. Therefore, the load is applied without impact effects, and it increases slowly and steadily until the fracture of specimen occurs. Even if quantitative precipitation difference can be detected microscopically, the overall difference is not enough to give rise to important modification in the movement of dislocation mechanisms and different strengthening of the matrix. So, the results of this quasi-static test are not affected by the different precipitation condition, because the dislocation are able to move in almost the same way in all samples.[40]

Therefore, the not-dependency of tensile property from one or two remelting process can be stated, at exception of elongation.

As for the tensile test results, the different precipitate content is not enough to affect hardness measurements carry out by a macroscopical indenter. Indeed, both Tukey's test of Brinell and Rockwell hardness do not show statistical difference between single-remelted samples and double-remelted ones, with very similar average values.

Another interesting aspect, which can be obtained from data analysis, is the relation between the mechanical properties and the remelting rate oscillation during the second stage of a VAR process. The plot of precipitates area fraction and some of the main mechanical properties (impact toughness, Yield strength 0.2 pct and elongation) *vs* the percentage standard deviation of the remelting rate are reported in Figure 13. The point dispersion is random for both single-remelted and double-remelted samples, therefore there is not any influence of the remelting rate on metallurgical properties of both VAR ingots. This means that the quality of ingots obtained is similar and, therefore, the trend of remelting rate does not influence the overall quality of the ingot.

V. SUMMARY

In this work, a characterization of Alloy 925 produced by EAF-AOD-VAR (single remelting) and EAF-AOD-VAR-VAR (double remelting) is realized. All samples considered are compliant with API 6ACRA standard,[2] but some considerations regarding final properties and the process can be done. Based on observations and results described in this work, the following conclusions can be stated:

1. The process parameters analysis of VAR process does not reveal differences between the two production ways. Therefore, the different behaviors of ingots produced with a single remelting can be correlated to defects derived from casting.
2. Single-remelted specimens have a general higher amount of titanium nitrides than double-remelted ingots. Moreover, the presence of titanium nitrides clusters is revealed only in the external position of single-remelted ingots. They may affect fatigue life of the material locally.
3. Single-remelted samples have a higher amount of intragranular precipitates respect to double-remelted. In particular, the amount increases from the center to the external zone (worst field), as expected from VAR process. Double-remelted ones have few precipitates in the external position.
4. Single-remelted samples have a higher amount of grain boundaries precipitates than double-remelted ones. It is probably due to lower removal of MC carbides produced by only single remelting.
5. Charpy test results (toughness and lateral expansion) are strongly reduced in single-remelted samples respect to double-remelted one. This is correlated to the higher amount of precipitates at grain boundaries.
6. Non-dependency of tensile test, at exception of elongation, and hardness on single or double VAR remelting is observed. The lower elongation of single-remelted samples is correlated to the higher presence of precipitates, which enhance the formation of voids.

Therefore, when a double remelting is not specifically required by a customer, a single-remelted ingot that satisfy the API 6ACRA standard requirements does not suffer of any severe decreasing in mechanical properties. Being the remelting rate slightly higher for a single remelting ingot, this can lead to an increase in productivity. By the way, the less cleanness of a single-remelted ingot must be taken into account because it can reduce toughness and fatigue resistance, slightly limiting the field of application of A925 forged components.

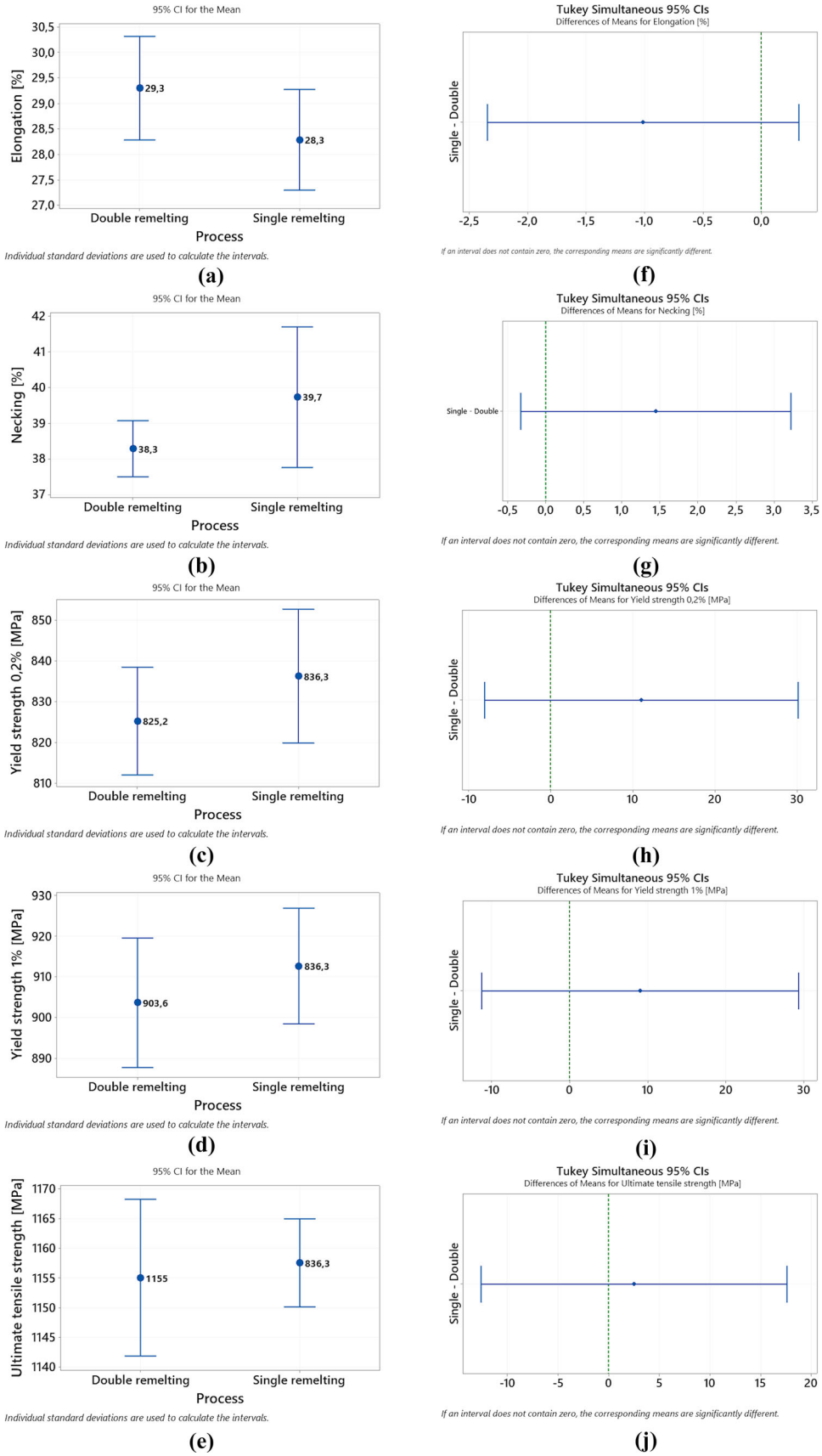

Fig. 12—Interval plot with individual standard deviation of elongation (*a*); necking (*b*); yield strength 0.2 pct (*c*); yield strength 1 pct (*d*); ultimate tensile strength (*e*); and HSD Tukey's test plot of elongation (*f*); necking (*g*); yield strength 0.2 pct (*h*); yield strength 1 pct (*i*); ultimate tensile strength (*l*).

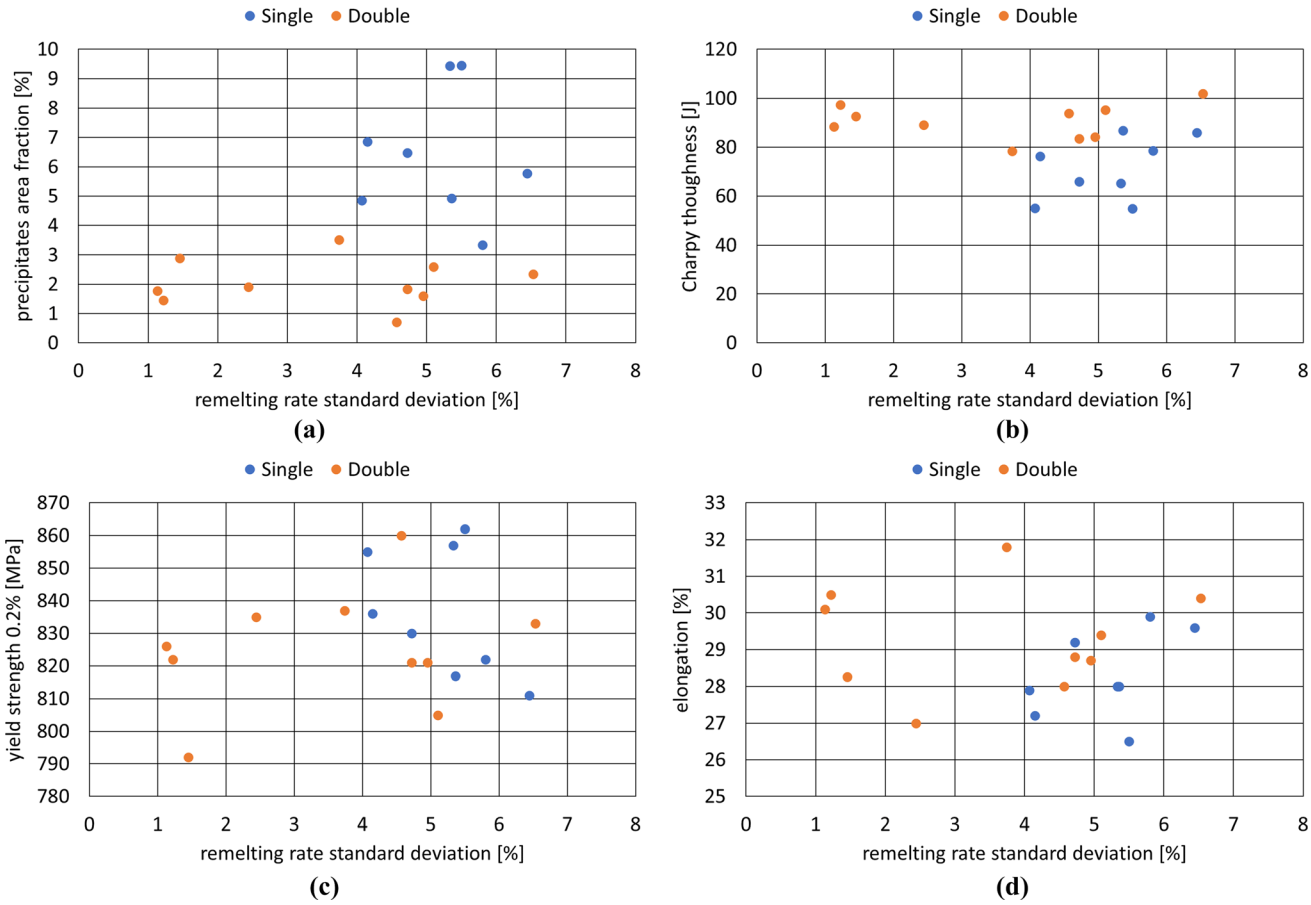

Fig. 13—Effect of remelting rate oscillation on precipitates area fraction (dev.st ± 0.25 pct) (*a*), Charpy impact toughness (dev.st ± 8.3 J) (*b*), yield strength 0.2 pct (dev.st ± 19 MPa) (*c*) and elongation (dev.st ± 1.9 pct) (*d*).

AUTHOR CONTRIBUTIONS

AD: formal analysis, investigation, data curation, writing—original draft. DM: methodology, visualization, writing—original draft. AG: validation, writing—review and editing. SB: resources. CM, AF, CV: conceptualization, supervision.

FUNDING

Open access funding provided by Politecnico di Milano within the CRUI-CARE Agreement. This research was supported by the Italian Ministry for Education, University and Research (MIUR) through the "Department of Excellence LIS4.0" project (Integrated Laboratory for Lightweight and Smart Structures).

CONFLICT OF INTEREST

The authors declare that they have no conflict of interest.

OPEN ACCESS

REFERENCES

1. Special Metals Corporation: INCOLOY (R) alloy 925, https://www.specialmetals.com/documents/technical-bulletins/incoloy/incoloy-alloy-925.pdf. Accessed 21 February 2022.
2. American Petroleum Institute: *API 6ACRA - Age-Hardened Nickel-Based Alloys for Oil and Gas Drilling and Production Equipment*, Washington (DC), 2018.
3. INTECO - special melting technologies GmbH: VAR-Vacuum Arc Remelting, http://www.gotrawama.eu/siderurgia/VAR Mail-version_2012-07-03.pdf. Accessed 21 February 2022.
4. A. Mitchell: *Mater. Sci. Technol.*, 2009, vol. 25, pp. 186–90.
5. R.L. Williamson, J.J. Beaman, D.K. Melgaard, G.J. Shelmidine, A.D. Patel, and C.B. Adasczik: *J. Mater. Sci.*, 2004, vol. 39, pp. 7161–68.

6. P.A. Davidson, X. He, and A.J. Lowe: *Mater. Sci. Technol.*, 2000, vol. 16, pp. 699–711.
7. J.R. Davis, ed.: *ASM Specialty Handbook: Nickel, Cobalt, and Their Alloys*, vol. 38, ASM International, Materials Park (OH), 2001.
8. W. Nicodemi and C. Mapelli: *Siderurgia*, 1st Edition, Milano, 2011.
9. In *ASM Handbook*, ASM International, Materials Park (OH), 2008, p. 1256.
10. P. Berthod, C. Vébert, L. Aranda, R. Podor, and C. Rapin: *Oxid. Met.*, 2005, vol. 63, pp. 57–72.
11. D.C. Montgomery: *Design and Analysis of Experiments, 8th Edition*, Wiley, New York, 2012.
12. D. Lane: Introduction to Statistics: Online Statistics Education: A Multimedia Course of Study, http://onlinestatbook.com/, Accessed 21 February 2022.
13. W. Zhang, P.D. Lee, and M. McLean: *in Intermetallics and Superalloys*, Wiley-VCH Verlag GmbH & Co. KGaA, Weinheim, FRG, 2006, pp. 121–28.
14. V. Descotes, T. Quatravaux, J.P. Bellot, S. Witzke, and A. Jardy: *Metals (Basel)*, 2020, vol. 10, p. 541.
15. P. Ganesan, E.F. Clatworthy, and J.A. Harris: *Corrosion*, 1988, vol. 44, pp. 827–35.
16. J.D. Busch, J.J. Debarbadillo, and M.J.M. Krane: *Metall. Mater. Trans. A Phys. Metall. Mater. Sci.*, 2013, vol. 44, pp. 5295–5303.
17. M. Rombouts, G. Maes, M. Mertens, and W. Hendrix: *J. Laser Appl.*, 2012, vol. 24, 052007.
18. L. Jiang, X. Ye, C. Cui, H. Huang, B. Leng, Z. Li, and X. Zhou: *Mater. Sci. Eng. A*, 2016, vol. 668, pp. 137–45.
19. J. Xie, J. Yu, X. Sun, T. Jin, and Y. Yang: *Jinshu Xuebao/Acta Metall. Sin.*, 2015, vol. 51, pp. 943–50.
20. D. Lei, T. Yang, B. Qu, J. Ma, Q. Li, L. Chen, and T. Wang: *Sustain. Energy*, 2014, vol. 2, pp. 1–4.
21. L. Jiang, W. Yinling, R. Hu, R. Liu, X.X. Ye, Z. Li, and X. Zhou: *Sci. Rep.*, 2018, vol. 8, p. 8158.
22. L. Jiang, W.Z. Zhang, Z.F. Xu, H.F. Huang, X.X. Ye, B. Leng, L. Yan, Z.J. Li, and X.T. Zhou: *Mater. Des.*, 2016, vol. 112, pp. 300–08.
23. H.K.D.H. Bhadeshia and R.W.K. Honeycombe: *Steels: Microstructure and Properties: Fourth Edition*, 3rd ed. Elsevier, Oxford, 2017.
24. Y.J. Shi, X.C. Wu, J.W. Li, and N. Min: *Int. J. Miner. Metall. Mater.*, 2017, vol. 24, pp. 1145–57.
25. A. Mondiere, V. Déneux, N. Binot, and D. Delagnes: *Mater. Charact.*, 2018, vol. 140, pp. 103–12.
26. H. Wang, D. Hong, L. Hou, P. Ou, Z. Wang, L. Shen, and H. Zhao: *Mater. Chem. Phys.*, 2020, vol. 255, 123554.
27. P. Li, D. Wu, C. Dai, X. Huang, C. Li, Z. Yin, S. Zhou, Z. Lv, D. Cheng, J. Zhu, J. Xu, and X. Liu: *Catal. Lett.*, 2019, vol. 149, pp. 1368–74.
28. F. Pan, W. Wang, A. Tang, L. Wu, T. Liu, and R. Cheng: *Prog. Nat. Sci. Mater. Int.*, 2011, vol. 21, pp. 180–86.
29. A.K. Jena and M.C. Chaturvedi: *J. Mater. Sci.*, 1984, vol. 19, pp. 3121–39.
30. S.S. Handa: University West, 2014.
31. X. Gao, L. Zhang, X. Chen, Y. Luan, and X. Qu: *Mater. Charact.*, 2020, vol. 167, 110492.
32. D. Texier, J. Cormier, P. Villechaise, J.C. Stinville, C.J. Torbet, S. Pierret, and T.M. Pollock: *Mater. Sci. Eng. A*, 2016, vol. 678, pp. 122–36.
33. G. Poojari, S.K. Kar, S.B. Singh, T.T. Kadavil, and C.R. Anoop: *Trans. Indian Inst. Met.*, 2019, vol. 72, pp. 1453–57.
34. A. Gramlich, T. Schmiedl, S. Schönborn, T. Melz, and W. Bleck: *Mater. Sci. Eng. A*, 2020, vol. 784, 139321.
35. S.Y. Chen and D. Gan: *Mater. Sci. Eng.*, 1986, vol. 84, pp. 65–76.
36. L.J. Wang, L.Y. Sheng, and C.M. Hong: *Mater. Des.*, 2012, vol. 37, pp. 349–55.
37. X.M. Chen, Y.C. Lin, M.S. Chen, H. Bin Li, D.X. Wen, J.L. Zhang, and M. He: *Mater. Des.*, 2015, vol. 77, pp. 41–49.
38. A. Loyda, L.A. Reyes, G.M. Hernández-Muñoz, F.A. García-Castillo, and P. Zambrano-Robledo: *Int. J. Adv. Manuf. Technol.*, 2018, vol. 97, pp. 2383–96.
39. W. Dai, Z. Yao, H. Zhang, C. Li, Y. Liu, and Y. Zhang: *J. Manuf. Process.*, 2022, vol. 76, pp. 291–303.
40. J.C. Stinville, E.R. Yao, P.G. Callahan, J. Shin, F. Wang, M.P. Echlin, T.M. Pollock, and D.S. Gianola: *Acta Mater.*, 2019, vol. 168, pp. 152–66.